Equation of state of water under negative pressure

Kristina Davitt,[a] Etienne Rolley, Frédéric Caupin, Arnaud Arvengas, and Sébastien Balibar
Laboratoire de Physique Statistique de l'Ecole Normale Supérieure, UPMC Université Paris 6, Université Paris Diderot, CNRS, 24 rue Lhomond, 75005 Paris, France

(Received 26 July 2010; accepted 10 September 2010; published online 2 November 2010)

We report on the simultaneous measurements of the speed of sound and the density in liquid water under negative pressure. Application of a focused acoustic wave to the bulk liquid is able to generate negative pressures before nucleation of the vapor phase occurs. A method for time-resolved Brillouin scattering is developed to measure the speed of sound during the passage of a 1 MHz ultrasonic wave. This is coupled with a fiber optic probe hydrophone which allows the determination of the density. Together, these methods give an ambient temperature equation of state of metastable liquid water down to the acoustic cavitation threshold. Empirical equations of state of water are based on experimental data at positive pressure; the validity of their extrapolation to negative pressures had been tested only indirectly or with very weakly metastable liquid. We provide thermodynamic data that prove the fidelity of recent equations of state down to −26 MPa. However, this raises questions regarding the nature of the cavitation threshold observed in acoustic experiments, which is far less negative than expected. © *2010 American Institute of Physics*. [doi:10.1063/1.3495971]

I. INTRODUCTION

There is no consensus on the equation of state of water. Liquid water exhibits many anomalies, such as a well-known density maximum at 4 °C and nonmonotonic behavior of thermodynamic properties such as the isothermal compressibility, which have yet to be fully explained. Highlights from recent computer simulation work evidence the large number of proposed models of water which attempt to account for this anomalous behavior.[1–5] In addition, numerous empirical equations of state (EOSs) have been developed and many faithfully represent liquid water under stable conditions, but predict qualitatively different behavior than simulations do in portions of the phase diagram that are less well characterized. This is particularly true for metastable states such as stretched water. If water is stretched by application of sufficiently large tensions, negative pressures can be attained. There is, however, a dearth of experimental data at negative pressures to support and test any proposed equations of state. The lack of data for a liquid of such ubiquity and importance as water is explained by the difficulty in obtaining the metastable state and subsequently measuring appropriate thermodynamic quantities. The aim of this work is to provide new thermodynamic data at negative pressures.

For a first order phase transition, an energy barrier must be overcome before the stable phase nucleates. In classical nucleation theory (CNT), this barrier arises from the balance between the energy cost of an interface separating the phases and a volumetric term favoring the production of the stable phase.[6] Due to this energy barrier, liquids can be stretched beyond the liquid-vapor equilibrium for a finite amount of time, in which case the liquid phase is metastable. However, in order to obtain this metastable state, extreme care must be taken to avoid surfaces and impurities which may reduce the barrier to nucleation, and consequently, the lifetime of the metastable state. Even without heterogeneous nucleation, a pure liquid has an absolute limit of stability, the liquid-gas spinodal line, beyond which the liquid phase is thermodynamically unstable. At the spinodal, the isothermal compressibility $\kappa_T = -1/V(\partial V/\partial P)_T$ diverges. In practice, thermal energy is sufficient to overcome the barrier to nucleation well before one reaches the spinodal. Thus, one does not have direct experimental access to the spinodal, but rather one measures a threshold which corresponds to a certain probability of cavitation within a specified experimental volume and time.[6,7] The cavitation threshold is thus a measure of the tensile strength of the liquid.

In water, knowledge of the cavitation threshold is of particular importance as its location is indicative of the spinodal[8] and may thereby aid in distinguishing between proposed EOS. For example, all molecular dynamics simulations find a spinodal that is monotonic with temperature,[9] whereas it has a minimum for extrapolations made from positive pressure data.[10]

This work was originally motivated by a longstanding discrepancy between experimental reports of the liquid-vapor cavitation threshold. Evaluating the disparity between experiments is complicated by the fact that the choice of measured variable, usually the cavitation pressure P_{cav} or density ρ_{cav}, depends on the method by which water is subjected to tension and conversion between them relies on the use of an extrapolated EOS. A recent review[11] summarizes the variety of methods that have been used to generate tension in water, and in recent experimental work[12] we provide a direct comparison between two of these methods. Knowledge of the EOS at negative pressures would enable com-

[a]Electronic mail: kristina.davitt@lps.ens.fr.

parison of existing reports of the cavitation threshold and verify the disparity; if it is real or if it is a product of an erroneous extrapolation.

Furthermore, as heterogeneous nucleation is difficult to avoid, interpretation of an experimental threshold is a perilous task. In contrast, it is expected that trace impurities have a minimal effect on continuous thermodynamic state variables, making comparison of experimental data throughout the negative pressure region a more trustworthy test of an EOS. In this communication, we measure two independent quantities from which the EOS can be obtained: the density ρ and the speed of sound $c^2=(\partial P/\partial\rho)_S$ at a known temperature. Before describing these measurements, we first briefly review the state of affairs with attention to those experiments that provide a measure or test of the EOS at negative pressures other than simply the cavitation threshold.

To our knowledge, the most extensive *PVT* measurements of water under mechanical tension were made by Meyer[13] almost a century ago. He used a combination Berthelot–Bourdon apparatus. A Berthelot tube consists of a sealed tube containing both liquid and vapor that is heated until all of the vapor condenses; the liquid can then be placed under tension by isochoric cooling.[14] The unwinding of a calibrated Bourdon tube gives a measure of the pressure. The liquid volume change upon the appearance of a vapor bubble is determined by measuring the bubble volume in a calibrated glass capillary and measuring the correction due to the contraction of the glass by submerging the entire apparatus in another liquid-filled vessel. Meyer was able to estimate κ_T; however, he could only obtain very weakly metastable states (-3.4 MPa) and found no significant deviation from the value at ambient pressure. Using the same method, however, he was successful in detecting curvature in $P(V)$ for the case of diethyl ether.[15]

Like Reynolds[16] and Briggs[17] before them, Winnick and Cho[18] used a centrifugal method to create a column of water under tension. In addition, they used the position of the meniscus to determine the density averaged over the column, and were able to make measurements down to roughly -10 MPa before cavitation occurred. However, interpretation of the results is difficult owing to the fact that the density is a function of position within the column and analysis necessitates a relation between P and ρ, implying that one is only able to test the consistency of the EOS employed. The original analysis has since been called into question[19] and revised[20] to conclude that more precise data and larger tensions are required.

Henderson and Speedy[21] were able to stretch water further, down to -20 MPa, before cavitation occurred. They used an apparatus similar to Meyer's to measure $P(T)$ curves and estimated V using an extrapolated EOS in order to determine the temperature of maximum density (TMD). Experimental measurement of the locus of TMD is particularly interesting in view of the stability limit conjecture,[10] but it can serve as a test of any EOS. The results are consistent with a number of EOS; Henderson and Speedy[21] concluded that their data were not sufficiently extensive.

The only known method to reach significantly higher tensions is the isochoric cooling of mineral inclusions. It is unclear why this method, and no other, is able to sustain such high tensions. The inclusion is akin to a microscopic-sized (≈ 10 μm) Berthelot tube. The measured variables are the temperature of disappearance of the vapor bubble, which is used to determine the density of the isochore using positive pressure data, and the temperature of cavitation. Measurements of the cavitation threshold[22,23] show considerable scatter, but have attained cavitation pressures down to -140 MPa. In one experiment, Alvarenga *et al.*[24] measured the speed of sound in inclusions using Brillouin scattering, concluded that nucleation occurs long before κ_T^{-1} is zero, and used an extrapolated EOS to find cavitation pressures that are consistent with predictions from CNT. No other thermodynamic data have been reported.

II. EXPERIMENTAL

Here we stretch water using an acoustic method. The acoustic wave compresses the liquid during the positive portion of oscillation and stretches it during rarefaction. The principal advantage of this method is that only a small volume of water is put under tension, for a short period of time, and far from any walls, thus reducing the influence of heterogeneous cavitation nuclei. As in previous studies,[25] we use a piezoelectric transducer in the form of a hemispherical shell (inner/outer diameters of 16/20 mm) to focus a high amplitude ultrasonic wave in water. The transducer is driven in bursts of 2 cycles at its resonance frequency of 1.06 MHz with a repetition rate of 300 Hz. The density and the speed of sound are measured during the passage of the acoustic wave at the focus of the transducer using two independent optical methods:

(i) a fiber optic probe hydrophone (FOPH), and
(ii) a time-resolved Brillouin scattering apparatus.

In the following sections, we separately describe the method of each measurement. Particular attention is paid to the challenging exercise of performing Brillouin scattering measurements during the passage of an acoustic wave, a task for which we have developed a relatively simple optical apparatus and careful timing control.

In both experiments, the volume of liquid involved is set by the size of the illuminated spot centered at the acoustic focus. The acoustic focus is a prolate ellipsoid with semiminor axes of 0.75 mm and a semimajor axis of 1.5 mm. The beam used for Brillouin scattering is focused to 35 μm, and the fiber probe has a core diameter of 50 μm. In both cases, this allows measurements over a region of the liquid where the pressure varies by less than 1% in space. Four notches machined into the edge of the transducer allow for optical access. These are used in the Brillouin experiment, whereas the fiber hydrophone is placed along the axis of cylindrical symmetry (see Fig. 1). The transducer is contained in a glass cuvette filled with ultrapure water produced by a commercial reverse-osmosis and UV lamp purification system. No additional degassing is done since the cuvette is closed but not hermetically sealed. The glass cuvette is surrounded by a copper enclosure followed by an insulating one, both with optical access, and the ensemble is temperature controlled.

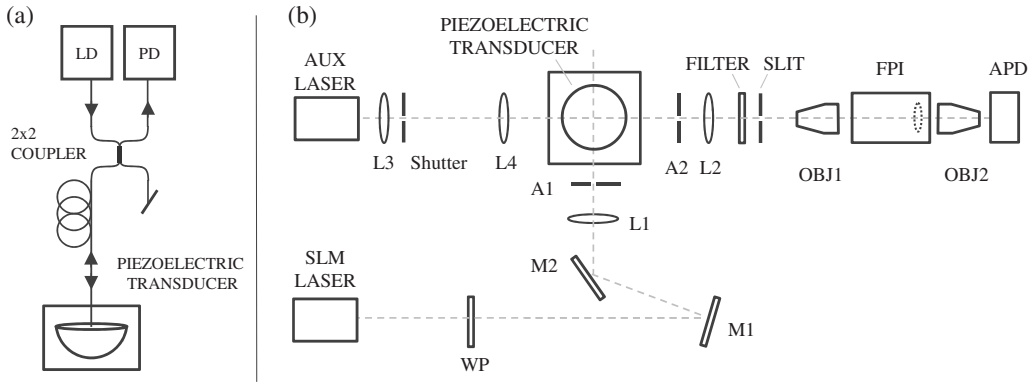

FIG. 1. (a) Side view schematic of the fiber optic probe hydrophone used for measurement of the density during passage of an acoustic wave. (b) Optical apparatus for the measurement of the speed of sound by Brillouin scattering, as seen from above. Optical components include a 1/2-wave plate (WP), simple lenses (L), mirrors (M), apertures (A), two objectives (OBJ), and an APD detector.

Over a 6 week period, the average temperature between experimental runs was kept at 23.30 ± 0.05 °C.

A. Brillouin scattering in an acoustic wave

Brillouin scattering is the inelastic scattering of light by thermal density fluctuations in a medium. The spectrum of scattered photons consists of an elastic Rayleigh peak surrounded by Brillouin satellites whose shift in frequency corresponds to the energy of emitted (Stokes) or absorbed (anti-Stokes) phonons. These spectra contain valuable information about the elastic properties of the medium.[26,27] There have been numerous studies of Brillouin scattering in water, including in the supercooled regime,[28,29] under high pressure and temperature,[30] as well as at high temperature in inclusions.[24] In this work, we use Brillouin spectra time-resolved during the passage of a 1 MHz acoustic wave to determine the speed of sound in water under negative pressure at ambient temperature.

The frequency-shift f_B of the Brillouin satellites with respect to the elastic peak is related to the speed of sound c in a medium of index of refraction n at a wavelength λ,

$$f_B = \frac{2nc}{\lambda}\sin\left(\frac{\theta}{2}\right), \tag{1}$$

where θ is the angle corresponding to a particular scattering wave vector. Precise measurements of f_B at this wave vector require the use of small in-plane numerical apertures. The Brillouin linewidth arises from damping terms and can be used to measure the absorption of sound.[26] Under ambient conditions of this experiment, f_B is 5.30 GHz and the full width at half maximum is approximately 300 MHz. The optical setup illustrated in Fig. 1(b) shows our experiments which were performed at 90°.

A 290 mW single longitudinal mode (SLM) 532 nm diode-pumped solid-state laser[31] is focused to a spot size of approximately 35 μm, coinciding with the acoustic focus. An aperture filters the beam, which is linearly polarized in the vertical direction before it enters the cuvette in order to maximize the Brillouin signal at the detector. A simple lens images the illuminated area to the plane of an adjustable vertical slit. A high-transmission 525 ± 25 nm bandpass filter inserted into the optical train reduces the background thought to be due to Raman scattering which, although smaller in peak intensity, can contribute a non-negligible amount of total intensity. A 10× objective collimates the beam before it enters a nominally 4 GHz free spectral range (FSR) piezo-scanned confocal Fabry–Perot interferometer (FPI) containing its own focusing lens.[31] The FPI is a common commercially available unit used with custom mirrors for increased transmission, which results in a finesse greater than 50. Light is extracted using a matching lens inserted into the housing of the FPI and refocused by a 32× objective to a 20 μm diameter avalanche photodiode (APD) exhibiting a dark count rate of 1 Hz. A photon counter is used to appropriately gate the APD to acquire counts only during an interval of 150 ns and at a variable delay Δt after triggering the transducer. The width of this window, hereafter referred to as the data channel, encompasses amplitudes within 10% of the peak of a focused 1 MHz acoustic wave. A DAQ counterboard serves as a second and slower channel, which is gated open for 1.75 ms between bursts to the transducer. This provides a reference at ambient pressure.

A spectrum is generated by scanning the FSR of the FPI with a linear voltage ramp composed of 500 discrete levels. At each step, a burst is sent to the transducer and the two time gates are opened following an appropriate delay. Owing to a weak scattered signal, the photon count rate at the Brillouin peak is 6500 s^{-1}. Thus, the majority of the 150 ns windows contain no counts. In order to construct a full spectrum with roughly 50 counts at the peak, 5×10^4 scans are required. However, the slower reference channel has a sufficiently long window to allow for the acquisition of a full spectrum after each scan of the FPI.

Two important considerations when using piezo-scanned instruments are the nonlinearity of the voltage-to-distance conversion and the well-known piezo-drift. The nonlinearity will be addressed in the analysis below. The drift phenomenon implies that returning to an original applied voltage does not ensure that the original position is recovered. This phenomenon must be contended with for any piezo-scanned FPI,[32] and we find it to be critical even for a confocal FPI since the accumulated drift is unpredictable and may be on the order of the FSR for long experiments. To compensate this drift, a feedback is used to apply a changing offset to the

voltage ramp such that the Brillouin peak of the reference channel is at a fixed position within the ramp. The feedback is updated approximately every 10 s. We note that the laser mode may also slowly drift. In any single experiment, it is not possible to distinguish between the laser and piezo-related drifts, but the feedback compensates both. From the observation that the drift depends highly on the scan conditions, we deduce that the piezos are the main source.

One experimental run results in a single data spectrum at a fixed Δt and takes roughly 15 h to acquire. The limiting factor in the speed of an experimental run is the maximum duty cycle of the high-voltage amplifier used to generate bursts to the piezoelectric transducer; here it is 0.1%. Specialized hardware, notably a multichannel photon counter with a sufficient readout speed, could significantly reduce the total experimental time by acquiring several spectra in parallel; we are not aware of any suitable commercial instruments at this time.

A primary difficulty of such a time-resolved Brillouin experiment is in aligning the incident laser beam with the acoustic focus. It is possible to use the diffraction of the beam by the acoustic wave for two directions and an auxiliary laser for the direction parallel to the excitation beam [shown in Fig. 1(b)]. However, it was found that location of the focus using the Brillouin signal itself yields a better accuracy. Thus, Brillouin maps of the acoustic field in three spatial dimensions and in Δt were made with at least three measurements in each dimension. In this manner, the acoustic focus is found with an estimated accuracy of 50 μm. This position is found to be consistent with the acoustic focus located using the FOPH, a much quicker procedure.

B. Fiber optic probe hydrophone

The time-varying density of water during passage of an acoustic wave is measured using a FOPH modeled on one originally developed by Staudenraus and Eisenmenger.[33] A detailed description of the FOPH apparatus applied to measurements of the density up to the cavitation threshold is outlined in a separate communication.[34] Briefly, modulation of the light intensity reflected from the cleaved facet of an optical fiber gives the modulation in the refractive index $n(t)$ of the liquid at the fiber tip,

$$R(t) = \left(\frac{n(t) - n_f}{n(t) + n_f}\right)^2, \tag{2}$$

where n_f is the index of the pure silica fiber core. The central component of the FOPH is a 3 dB 2×2 step-index fiber optic coupler, with a 808 nm laser diode located at one input port, the bare fiber tip (cleaved at 90°) of one output port located at the acoustic focus in the liquid, and a silicon photodiode at the other input to measure the light reflected back into the coupler. Figure 1(a) shows a sketch of the apparatus. To calculate the density from the refractive index, a semiempirical formula based on the Lorentz–Lorenz relation[35] is used. When extrapolated over the range of densities obtained here, this relation is linear to better than 1%. Two corrections to this basic model are allowed for. First, a stray-light term is included to account for any reflection from the unused arm of the coupler and the nonzero crosstalk of the coupler itself. This quantity is measured using a series of calibrated microscope immersion oils.[34] Second, and of more consequence, a correction is made to allow for the compressibility of the optical fiber. The latter amounts to a pressure-dependent fiber index, $\partial n_f/\partial P$. This correction can be approximated by

$$n_f(t) = n_f(0) + [n(t) - n(0)]\frac{\partial n_f}{\partial P}\frac{\partial \rho}{\partial n}c^2, \tag{3}$$

where $t=0$ corresponds to no acoustic wave. For the purposes of this correction term, $t=0$ values are used for the speed of sound c and the refractive index of water as a function of density.[35] We note that $\partial n_f/\partial P$ will be estimated in the experiments presented here by using the positive pressure equation of state data.

C. Combination

Before each experimental run, the ultrapure water was replaced and the transducer drive voltage was set to a constant value corresponding to 80% of the cavitation threshold. Here we define the cavitation threshold as the point at which the probability of cavitation—detected from the echo of the resulting vapor bubble—is one half. Owing to the double-exponential form of the probability of a thermally driven cavitation process, at 80% of the threshold there are essentially no bubbles. The statistics of cavitation in water was the subject of a previous study,[25] where it was shown that the acoustic cavitation threshold is extremely reproducible and depends only weakly on the gas content. The Δt was set to be consistent with the time-of-flight of an acoustic wave across the radius of the transducer. Dedicated software synchronized all timed events and recorded intermediate Brillouin spectra roughly every 10 s. FOPH measurements were made systematically at the end of each run.

III. RESULTS AND ANALYSIS

The raw output from FOPH and Brillouin scattering experiments are the reflection as a function of time $R(t)$ and a series of time-resolved spectra. To determine the speed of sound and density at an instant in the acoustic wave, both data are required. First, we describe the analysis of each measurement independently. Following, we use both measurements to compare to well-known positive pressure $c(\rho)$, and thereby extract the correction term $\partial n_f/\partial P$ for the compressibility of the fiber hydrophone. Finally, we use this correction to determine the behavior at negative pressures.

A. Brillouin spectra

Any spectrum acquired using a piezo-scanned FPI must have the frequency axis calibrated to account for the nonlinear relation between the applied voltage and the FPI resonance frequency. One way to do so is to use a set of reference peaks of known frequency. During our experiment, we repeatedly scan the FPI over a little more than one free spectral range and thus have four peaks in each reference scan; a Stokes and anti-Stokes Brillouin peak (B_1, B_2) and two elastic peaks (E_1, E_2) from each end of the FSR. Below, we

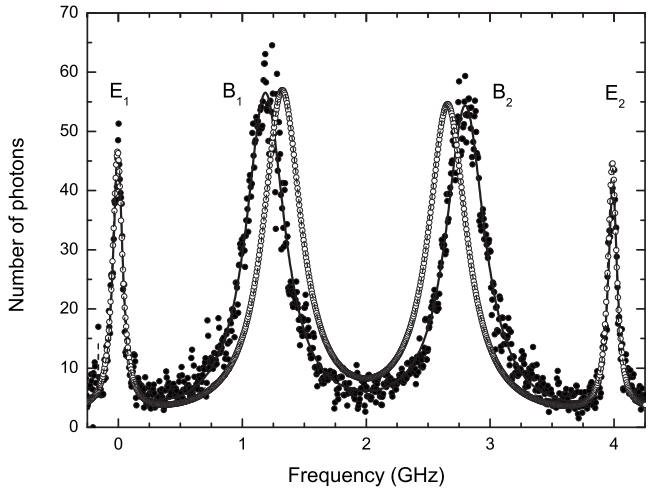

FIG. 2. Results from a single Brillouin run. The data spectrum (closed circles) is acquired during a window of 150 ns around the maximum tension and the reference spectrum (open circles) between acoustic bursts. The latter has been scaled here and both have been fit by the form in Eq. (4).

outline a procedure that uses the reference scans to generate a conversion to calibrate the frequency scale.

The four peak positions in each reference scan are located using a six Lorentzian peak fit form with 12 fitting parameters,

$$I(f) = \sum_{i=1,2} \frac{I_{B_i}}{1+4\dfrac{(f-f_{B_i})^2}{\Gamma_{B_i}^2}} + \sum_{i=1,2} \frac{I_{E_i}}{1+4\dfrac{(f-f_{E_i})^2}{\Gamma_{E_i}^2}} + \frac{I_{B_1}}{1+4\dfrac{(f-\mathrm{FSR}-f_{B_1})^2}{\Gamma_{B_1}^2}} + \frac{I_{B_2}}{1+4\dfrac{(f+\mathrm{FSR}-f_{B_2})^2}{\Gamma_{B_2}^2}}, \tag{4}$$

where I is the peak intensity and Γ is the full width at half maximum of each peak. The first sum corresponds to the Brillouin satellites whose fundamental lineshape is Lorentzian[26,36] apart from a small asymmetric term,[36,37] which we neglect here. The second sum corresponds to the elastic peaks, which are approximately Lorentzian since the laser linewidth of 1 MHz is broadened by the modest finesse of the FPI. Here, the Brillouin satellites are sufficiently wide that the tail of the peak in the next FSR beyond the scan influences the baseline (see Fig. 2). To account for this, we include two additional peaks which are shifted copies of the Brillouin satellites [last two terms in Eq. (4)]. To reduce the effect of the error in individual fits, the position of each of these peaks as a function of the scan number n is then smoothed by fitting to a third-order polynomial. Finally, the smoothed positions are fitted with a second-order polynomial in the voltage $f=\alpha(n)+\beta(n)V+\gamma(n)V^2$, where the coefficients are determined using $f_{E_1}=0$ and $f_{E_2}=\mathrm{FSR}$,[38] and by forcing the Stokes and anti-Stokes shifts to be equal, $f_{B_1}=\mathrm{FSR}-f_{B_2}$. The result of such a procedure is to produce a voltage-to-frequency conversion for each scan; it is general enough that it allows for the possibility of a conversion that varies slowly with the offset voltage applied to the piezos. All other constants in Eq. (1) are known for the reference channel, so f_B may be used to find the precise θ of the setup; here it is 90.16°. The same coefficients are then applied to the data channel and the individual scans are summed. Figure 2 shows the resulting data spectrum acquired at the maximum tension compared to the reference spectrum acquired during the same experiment. The corrected data spectrum, which has roughly 50 photons at the Brillouin peak, is then fit to the form in Eq. (4). The quantity of interest is the shift in f_B between the data channel and the reference channel,

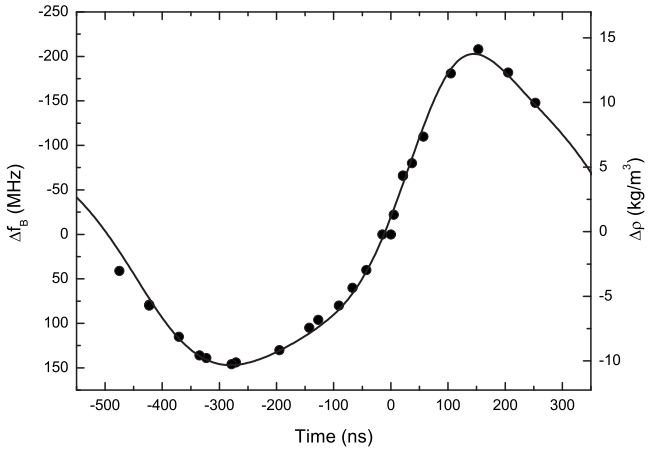

FIG. 3. Change in Brillouin shift (filled circles) and in density (solid line) during passage of a 1 MHz acoustic wave in water.

$$\Delta f_B = \tfrac{1}{2}(f_{B_1}^{\mathrm{data}} + f_{B_2}^{\mathrm{data}} - f_{B_1}^{\mathrm{ref}} - f_{B_2}^{\mathrm{ref}}). \tag{5}$$

An uncertainty of 5 MHz in Δf_B results from the error in finding the peak position in a Brillouin satellite with Poissonian noise. Figure 3 shows the resulting Δf_B measured over 1 cycle at the acoustic focus.

B. FOPH

To determine the density of water from the reflection measured by the FOPH, we first calculate the index of refraction using Eqs. (2) and (3), assuming the compressibility of the fiber $\partial n_f/\partial P$ is known. A semiempirical formulation is then used to relate the index and density.[35] In using the latter, we assume that the temperature is constant within the acoustic wave. However, strictly speaking, it follows an isentropic.[34] Using an extrapolated EOS,[39] we estimate the temperature change within the acoustic wave to be <0.6 °C over the range of densities measured here. This introduces a worst-case error in the density of ± 0.04 kg m^{-3}, smaller than our measurement uncertainty which we estimate to be ± 0.7 kg m^{-3} from statistical reproducibility of the threshold. Finally, to compare the instantaneous FOPH measurement to Brillouin spectra, which are acquired over a 150 ns integration time, the FOPH signal is processed by a boxcar moving average with the same time window. Figure 3 shows the resulting modulation in the density during the acoustic wave. The measured waveforms are not sinusoidal due to the nonlinear response of the high-voltage amplifier to a 2-cycle burst, which is further exaggerated by nonlinearities in the sound wave.

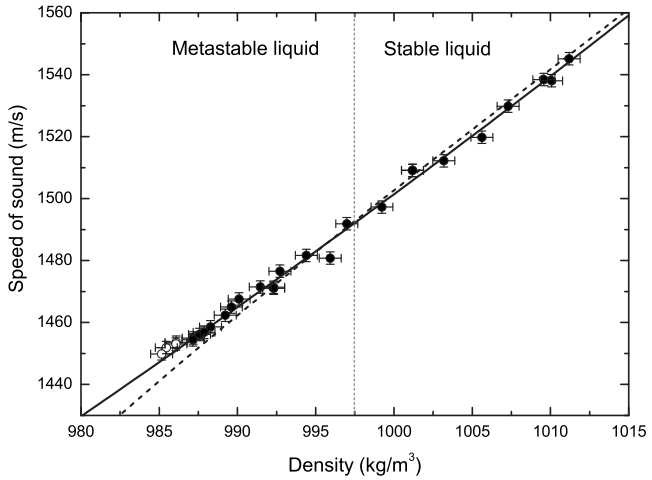

FIG. 4. Speed of sound as a function of density for both water under tension (left) and under pressure (right). Filled circles are the data taken with the transducer drive at 80% of the cavitation threshold, and open circles are with higher excitation. Solid/dashed lines are calculated from the IAPWS and HGK EOS, respectively.

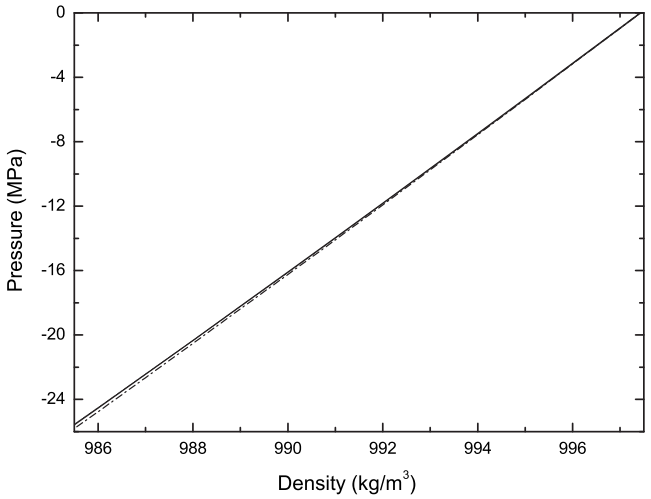

FIG. 5. Equation of state of water at 23.3 °C over the range of negative pressures accessible to acoustic experiments. The experimental result obtained using Eq. (6) (dashed-dotted line) is compared to the theoretical predictions from the IAPWS and HGK EOS, which are indistinguishable on this scale (solid line).

C. Positive pressure

To determine c at a point in time during the acoustic wave using Eq. (1), one needs both the shift Δf_B from the Brillouin experiment and the corresponding index of refraction n from the FOPH. One can then determine $c(\rho)$, which is well-known at positive pressures. However, as discussed in detail in Ref. 34, precise literature values for the compressibility of the fiber are lacking. Instead, we use our experimental data taken at positive pressure to determine $\partial n_f/\partial P$. Data during the compression phase of the acoustic wave in Fig. 3 are fit to known[40] $c(\rho)$ with two adjustable parameters: $\partial n_f/\partial P$ and a time delay between the FOPH and Brillouin experiments that allows for a small synchronization offset. The resulting best-fit is shown on the right hand side of Fig. 4, where $\partial n_f/\partial P$ is $(10.6\pm3)\times10^{-6}$ MPa^{-1}. This value lies within the range reported for pure silica: from 5 to 14.2×10^{-6} MPa^{-1} (see references within Ref. 34).

D. Negative pressure

For data during the rarefaction phase of the acoustic wave, $c(\rho)$ is found using the compressibility of the fiber determined above. Results are shown as filled circles in the left hand side of Fig. 4. These experiments were performed at 80% of the cavitation threshold and reached a density of 987.15 kg m^{-3} around the acoustic wave minimum. For comparison, one can use a common empirical EOS[39] to calculate the corresponding average pressure over the 150 ns count window: −22 MPa. To access higher tensions, one can increase the drive to the transducer to approach the cavitation threshold. There are two practical inconveniences to this: cavitation events can destroy the end face of the fiber (which must then be recleaved), and bubbles have a large elastic scatter which overwhelms the Brillouin signal. We have incrementally increased the drive to the transducer to 95% of the threshold, shown as open circles in Fig. 4, using the same analysis procedure but removing scans where at least one bubble was present. Bubbles are easily identified by the large elastic scatter arising from the reflection of the laser beam at the liquid-vapor interface. In this case, the minimum speed of sound and density reached were 1449.9 m s^{-1} and 985.2 kg m^{-3}, corresponding to an average pressure of −26 MPa. We note that slightly more negative pressures can be obtained using a higher frequency sound wave.[34] This is due to the smaller volume and shorter duration of the applied tension which, as predicted by nucleation theory, results in a more negative cavitation threshold. However, the very modest gain in pressure must be weighed against the increased experimental difficulty of operating in small volumes and short times.

IV. DISCUSSION

Shown in Fig. 4 are $c(\rho)$ calculated from the IAPWS (Ref. 39) and HGK (Ref. 41) scientific equations of state. Both of these empirical equations have a physical basis and are framed in terms of the Helmholtz free energy as a function of temperature and density. The former is the most recent international formulation. The older HGK EOS is included for comparison as it was used in earlier works involving water under negative pressure.[22] The difference between them in the stable liquid region is within their stated estimates of certainty. It is important to note that the use of any EOS for metastable water at negative pressures constitutes an extrapolation for which little supporting data exist. Now, the experimental results in Fig. 4 provide support for the extrapolation of both of these EOSs over the full range of accessible tensions. The slight curvature seen at the most negative pressures appears to favor the IAPWS formulation. We note that the analysis to determine the fiber compressibility uses positive pressure data[40] derived from IAPWS. However, if the HGK EOS is used instead, the experimental data shift by less than the indicated error bars.

One can go a step further and integrate the speed of sound and density data to determine the EOS in the usual $P(\rho)$ plane. Figure 5 shows both isotherms from the two

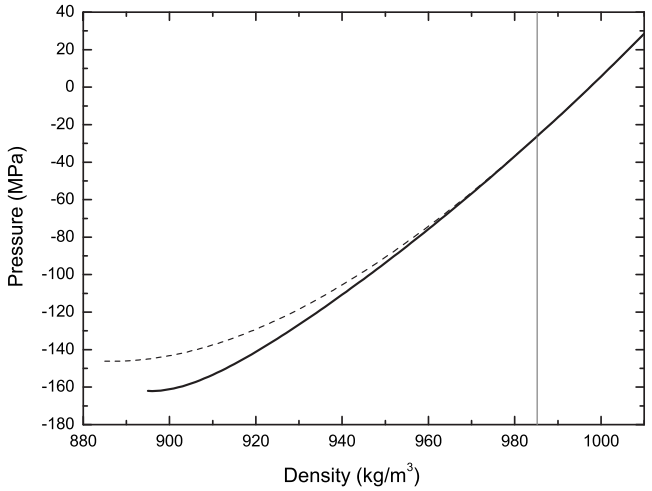

FIG. 6. Equations of state of water at 23.3 °C from the IAPWS (solid line) and HGK (dashed line) formulations extrapolated to their spinodal pressures. The range of pressures reached in acoustic experiments is limited to the right hand side of the vertical line.

empirical EOS and one determined from our results. We have obtained the latter by fitting the $c(\rho)$ data to a second-order polynomial and neglecting the difference between an isotherm and an isentropic, which we justify for pressures obtained here with arguments made in Sec. III B,

$$c = \sqrt{\left(\frac{\partial P}{\partial \rho}\right)_S} \approx \sqrt{\left(\frac{\partial P}{\partial \rho}\right)_T} = a_0 + a_1\rho + a_2\rho^2. \quad (6)$$

This matches the theoretical predictions to be better than 2% over the range of measurement, confirming that the extrapolated EOS faithfully represents water stretched down to −26 MPa. Furthermore, these results provide a constraint at negative pressures that must be applied to any new EOS.[42]

This conclusion was not *a priori* evident. In fact, to explain the discrepancy between experimental reports of the liquid-vapor cavitation threshold, some of which measure ρ_{cav} and others P_{cav}, it was suggested that the use of an EOS extrapolated beyond its limits of validity could erroneously introduce a difference.[25] This no longer appears plausible, certainly for cavitation thresholds near −30 MPa. One must keep in mind, however, that the approximation and polynomial fit made above are not reliable beyond this limit. However, we are unable to access higher tensions because the liquid systematically cavitates. This raises two key questions: (1) how can the discrepancy in cavitation thresholds be explained and (2) how can the EOS of water under larger negative pressures be measured experimentally.

Using the FOPH, we have measured the cavitation density and statistics[12] from which we can now confidently calculate $P_{cav}=-28.7\pm1.5$ MPa at 23.3 °C. This is consistent with the majority of reports of the cavitation pressure in pure water.[11] In contrast, our cavitation threshold (vertical line in Fig. 6) is far from the calculated spinodal. In fact, the divergence of κ_T in the IAPWS and HGK EOSs predicts $P_s \approx -160$ and −140 MPa, respectively. Indeed, only in mineral inclusions have such high tensions been observed in water, and P_{cav} near −140 MPa at 39.9 °C have been reported.[22] One might then question whether heterogeneous nucleation is at play in all other experiments including the present one; however, this is contrary to the remarkable reproducibility of the threshold for acoustic cavitation, a method in which the full statistics of cavitation are easily accessible and well studied.[25,43] One can only speculate on other reasons for the discrepancy in the cavitation thresholds. We have recently proposed[12] that fundamental impurities, such as hydronium ions naturally present in neutral water, could be centers for nucleation, which would be absent or inactivated in some quartz inclusions. Alternatively, due to the high pressure and temperature needed to synthesize quartz inclusions, silica could be present in water and increase its tensile strength. We have also considered how the presence of a metastable liquid-liquid critical point at negative pressure could cause the cavitation threshold to depend on the thermodynamic path followed to place water under tension. However, the latter proposal is doubtful in light of recent work. Indeed, there is currently no satisfactory explanation for the apparently low cavitation threshold in all experiments other than inclusions.

The experimental reality appears to be that only in mineral inclusions can higher tensions be observed. Thus, to measure the EOS of water at more negative pressure, further experiments must be performed by applying tension in this way. The difficulty with this method lies in making measurements of at least two independent variables from which the EOS may be determined, as was done here for the acoustic method. In inclusion studies reported to date, one must rely on the assumption that the host material does not deform and thus that the experiment is done under isochoric conditions. The development of techniques to simultaneously measure two independent variables in inclusions would eliminate the need for this assumption. We suggest that this would be fruitful in further elucidating the EOS of water under tension and may shed light on why a larger range of metastability can be achieved when water is stretched in mineral inclusions.

Another possibility is to extend current measurements to other temperatures, and in particular, to near the freezing point where other experiments[12] have hinted at a small deviation from extrapolated EOS. This would necessitate thermal insulation of the optical cell to prevent condensation on the surrounding optics and is not expected to reach significantly lower pressures.

In this work, we measured the speed of sound using the Brillouin shift. In addition to the shift, the peak width and the relative intensity of the Brillouin and Rayleigh peaks contain valuable information about additional thermodynamic quantities. The elastic component of molecular scattering in water is very small,[44] with a minimum at 4 °C, and water is notoriously difficult to keep pure enough to measure this component in a background of elastic scatter from impurities. In the experiments described here, the elastic scatter varies from scan to scan, presumably due to particulate matter that passes through the optical focus. We also observe a slow increase in the average elastic peak height during the experiment, the origin of which is unknown. Here a small amount of stray light is necessary to the analysis in order to have four clear peaks within the FSR with which to calibrate the frequency scale; however, this renders impossible the determination of

the relative peak intensity. Nevertheless, the fundamental linewidth of the Brillouin satellites is accessible after correcting for experimental broadening effects arising from the numerical aperture of the collection optics, the finite finesse of the FPI, and the feedback to compensate the piezo-drift. The last two are contained in the linewidth of the elastic peaks after summing all scans, from which we find an effective finesse of approximately 50. The first effect can be estimated from the $\pm 3°$ collection angle, which was chosen to maintain a reasonable signal intensity. It is important to note that broadening is symmetric around 90°, so a nearly Lorentzian lineshape is maintained. After deconvolution, the average linewidth is 280 MHz. The dispersion over all measurements is ± 25 MHz. Calculating the sound absorption following Ref. 29 yields an average of $\alpha/f^2 = 21 \times 10^{-15}$ s^2 m^{-1}. This value is consistent with previous reports at ambient pressure.[28,29,45] It is interesting to measure the absorption of sound as a divergence of this quantity may be indicative of the approach of a thermodynamic instability or a critical point.[46] For water stretched down to the acoustic cavitation threshold, we did not find any dependence on the pressure within the experimental scatter. It would be interesting to extract the absorption of sound from Brillouin scattering measurements in inclusions to search for a divergence at more negative pressures.

V. CONCLUSION

We have built a Brillouin scattering apparatus and a fiber optic probe hydrophone to measure the speed of sound and the density of water during application of an ultrasonic wave. The relatively simple optical setup and analysis procedure developed for Brillouin scattering may be used to take time-resolved spectra on the nanosecond scale of any repeatable process. We have combined these two optical measurements to investigate the behavior of water under tension down to -26 MPa. To our knowledge, such thermodynamic data have never been reported in this part of the phase diagram for liquid water. We find that the experimental results are fitted well by extrapolation of the recent IAPWS formulation for the equation of state.

ACKNOWLEDGMENTS

We thank T. Greytak, P. Jacquier, J. Dupont-Roc, and H. J. Maris for discussions in the early stages of the experiment. This research has been funded by the ERC under the European Community's FP7 Grant Agreement No. 240113.

[1] P. G. Debenedetti and H. E. Stanley, Phys. Today **56**(6), 40 (2003).
[2] C. A. Angell, Science **319**, 582 (2008).
[3] H. Stanley, P. Kumar, G. Franzese, L. Xu, Z. Yan, M. Mazza, S. Buldyrev, S.-H. Chen, and F. Mallamace, Eur. Phys. J. Spec. Top. **161**, 1 (2008).
[4] I. Brovchenko and A. Oleinikova, ChemPhysChem **9**, 2660 (2008).
[5] K. Stokely, M. Mazza, H. Stanley, and G. Franzese, Proc. Natl. Acad. Sci. U.S.A. **107**, 1301 (2010).
[6] P. G. Debenedetti, *Metastable Liquids* (Princeton University Press, Princeton, 1996).
[7] H. J. Maris, C. R. Phys. **7**, 946 (2006).
[8] F. Caupin, Phys. Rev. E **71**, 051605 (2005).
[9] P. G. Debenedetti, J. Phys.: Condens. Matter **15**, R1669 (2003).
[10] R. J. Speedy, J. Phys. Chem. **86**, 982 (1982).
[11] F. Caupin and E. Herbert, C. R. Phys. **7**, 1000 (2006).
[12] K. Davitt, A. Arvengas, and F. Caupin, EPL **90**, 16002 (2010).
[13] J. Meyer, Abhandl. d. Deutsch Bunsen-Gessellschaft **6**, 1 (1911).
[14] M. Berthelot, Ann. Chim. Phys. **30**, 232 (1850).
[15] J. Meyer, Zeitschrift Für Elektrochemie **17**, 743 (1911).
[16] A. M. Worthington, Philos. Trans. R. Soc. London Ser. A **183**, 355 (1892).
[17] L. J. Briggs, J. Appl. Phys. **21**, 721 (1950).
[18] J. Winnick and S. J. Cho, J. Chem. Phys. **55**, 2092 (1971).
[19] J. R. Macdonald, J. Chem. Phys. **57**, 3793 (1972).
[20] H. S. Huang, D. L. Guell, and J. Winnick, J. Chem. Phys. **59**, 6191 (1973).
[21] S. J. Henderson and R. J. Speedy, J. Phys. Chem. **91**, 3062 (1987).
[22] Q. Zheng, D. J. Durben, G. H. Wolf, and C. A. Angell, Science **254**, 829 (1991).
[23] K. I. Shmulovich, L. Mercury, R. Thiéry, C. Ramboz, and M. El Mekki, Geochim. Cosmochim. Acta **73**, 2457 (2009).
[24] A. D. Alvarenga, M. Grimsditch, and R. J. Bodnar, J. Chem. Phys. **98**, 8392 (1993).
[25] E. Herbert, S. Balibar, and F. Caupin, Phys. Rev. E **74**, 041603 (2006).
[26] I. Fabelinskii, in *Progress in Optics*, edited by E. Wolf (Elsevier, Amsterdam, 1997), Vol. 37, Chap. 3, pp. 95–184.
[27] B. Chu, *Laser Light Scattering* (Academic, New York, 1974).
[28] J. Rouch, C. Lai, and S. Chen, J. Chem. Phys. **65**, 4016 (1976).
[29] J. Teixeira and J. Leblond, J. Physique Lett. **39**(7), 83 (1978).
[30] M. Grimsditch, S. Popova, and A. Polian, J. Chem. Phys. **105**, 8801 (1996).
[31] The SLM diode laser model Torus was purchased from Laser Quantum Ltd. (UK). Active mode-locking is turned off during measurement to eliminate the effective bandwidth broading caused by the feedback. The FPI is a standard model FPI-100 from Toptica Photonics (Germany) used with custom mirrors having 99.2% reflectivity at 532 nm.
[32] J. Sandercock, J. Phys. E **9**, 566 (1976).
[33] J. Staudenraus and W. Eisenmenger, Ultrasonics **31**, 267 (1993).
[34] A. Arvengas, K. Davitt, and F. Caupin (unpublished).
[35] The International Association for the Properties of Water and Steam, Release on the Refractive Index of Ordinary Water Substance as a Function of Wavelength, Temperature and Pressure (1997).
[36] W. Nichols and E. Carome, J. Chem. Phys. **49**, 1000 (1968).
[37] O. Conde, J. Leblond, and J. Teixeira, J. Phys. France **41**, 997 (1980).
[38] We calibrated the FSR by taking Brillouin spectra at ambient pressure and changing the water temperature between 20 and 30 °C. The FSR is adjusted such that the expected shift, calculated from known $c(T)$ (Ref. 39), is obtained. The result differs by only -0.5% from the nominal FSR.
[39] The International Association for the Properties of Water and Steam, Revised Release on the IAPWS Formulation 1995 for the Thermodynamic Properties of Ordinary Water Substance for General and Scientific Use (2009).
[40] P. Linstrom and E. W. G. Mallard, NIST Chemistry WebBook, NIST Standard Reference Database Number 69 (National Institute of Standards and Technology, Gaithersburg, MD, retrieved 13 June 2010) p. 20899, http://webbook.nist.gov.
[41] J. Kestin, J. Sengers, B. Kamgar-Parsi, and J. L. Sengers, J. Phys. Chem. Ref. Data **13**, 175 (1984).
[42] The best-fit coefficients to Eq. (6) are $a_0 = 1.297743627 \times 10^4$, $a_1 = -2.666568 \times 10^1$, and $a_2 = 1.519 \times 10^{-2}$; See supplementary material at http://dx.doi.org/10.1063/1.3495971 for the raw data from Fig. 4.
[43] E. Herbert, "Cavitation acoustique dans l'eau pure," Ph.D. thesis, Université Paris 7-Denis Diderot, 2006.
[44] H. Cummins and R. Gammon, J. Chem. Phys. **44**, 2785 (1966).
[45] J. Ostwald, W. Pazold, and O. Weis, Appl. Phys. (Berlin) **13**, 351 (1977).
[46] R. J. Speedy and C. A. Angell, J. Chem. Phys. **65**, 851 (1976).